www.rericjournal.ait.ac.th

Simulation of the Power Electronic Device based on MMC Structure

Yongwei Tang*, Maoli Wang*, +, 1, Huijuan Hao*, and Xiaojie Zhao*

Abstract – *In this paper, the topology of power electronic transformer based on modular multilevel converter (MMC) structure was studied firstly. And a new topology was proposed that combines the power electronic transformer with energy storage system. Then, the control strategy of power electronic transformer was introduced. Finally, the simulation model of power electronic transformer based on MMC structure was built in PSCAD simulation environment. The simulation results showed that the power electronic transformer is able to ensure the voltage and current waveform of the input and output side in sinusoidal, resist load disturbance, isolate fault and isolate harmonic propagation. In addition, the battery model was also studied in PSCAD simulation environment, followed with the analysis of the influence of battery energy storage on load. The power electronic transformer topology with energy storage system proposed in this paper can guarantee both the quality and the reliability of power supply.*

Keywords – energy storage system, MMC, power electronic transformer, simulation analysis, topology.

1. INTRODUCTION

The construction of smart grid plays an important role in the reorganization of energy structure and improvement of the environment. The study on highly-intelligent electrical equipment could significantly advance the construction of smart grid. The development of smart grid has also introduced the power electronic transformer (PET) that not only possesses the functions of the traditional transformer, but also adopts proper control strategies to ensure the primary and secondary voltage and current waveforms in sinusoidal. Meanwhile, the presence of PET DC bus brings convenience to the access of distributive energy.

PET meets the need of smart grid's future development and the analysis of the PET's characteristics of PET facilitates a better application of PET. Literature [2] pointed out that AC/AC topologies have low PET controllability and small application value. The existing studies mainly focus on AC/DC/AC PET. Literature [3], [4] studied the cascaded H-bridge PET topology, but the topology required more high-frequency transformers and power electronic devices compared to the MMC structure, appearing to be not cost-effective enough. Literature [5] proposed the new PET topology based on MMC structure and verified the proposed topology and the feasibility of the control strategy; Literature [6] studied the PET topology of the MMC structure and verified the functions of PET transforming and power quality regulation; Literature [7] proposed an internal model control method for MMC-structured PET, and simulated the anti-load disturbance capability of PET. However, none of the above studies dived into the isolated fault and harmonic wave propagation function of MMC-structured PET. Besides, when PET is used as a distribution transformer, its area often carries a load that requires high reliability of power supply. Therefore, it is often necessary to configure the energy storage. The above literatures didn't consider the combination of PET and energy storage technology in the study of MMC-structured PET. So far, there have been few literatures engaging the combination of PET and energy storage. Literatures [8] and [9] studied the PET with the energy storage system and the energy storage module adopted supercapacitor energy storage that cost huge and now could only be applied to a small range as more time is needed before wider application.

Firstly, the paper first introduced the PET topology based on MMC structure, according to which, a topological structure combining lithium battery energy storage with PET was proposed. Then the control strategies adopted at all levels of PET were elaborated. In the PSCAD simulation environment, it was verified that the MMC-based PET could ensure the voltage and current waveform at the input and output sides in sinusoidal, resist load disturbance, isolate fault and isolate harmonic propagation. In addition, the lithium battery was modelled in the PSCAD environment, and the impact of the lithium battery on the load power supply was also studied. The MMC-based PET combined with the energy storage can guarantee both the quality and reliability of power supply, which is of noticeable research significance.

2. TOPOLOGY

What this paper studied is a new type of MMC-structure-based PET topology that has combined the existing PET topology and the energy storage

*Shandong Provincial Key Laboratory of Computer Networks, Shandong Computer Science Center (National Supercomputer Center in Jinan), Qilu University of Technology (Shandong Academy of Sciences), Jinan 250014, China.

+Key Laboratory of Power System Intelligent Dispatch and Control of the Ministry of Education, Shandong University, Jinan 250061, China.

1 Corresponding author;
E-mail: wangml@sdas.org.

technology to be applied to the medium and high voltage distribution network, as shown in Figure 1. The combination of energy storage system and PET could ensure the sufficient power supply of the load when the input stage voltage interrupts or drops deep [8], [9]. Different from the supercapacitor energy storage proposed in Literature [8], [9], the energy storage device used in this paper is lithium battery energy storage. Except for the advantages of large capacity, high energy density, high energy conversion efficiency and long life, the technology of lithium battery has been also developed mature enough [10], and the MW-level demonstration projects could be found both at home and abroad. Literature [11] mentioned the comprehensive functions of PET to realize the demand-based electricity supply by integrating PET into new energy generation, energy storage system, electric vehicle and load. In the overall application of PET, the choice of energy storage device has become particularly important. The lithium battery energy storage is able to help grid to stabilize the fluctuation and smoothen the new energy power output, indicating a broad application prospect in the field of smart grid.

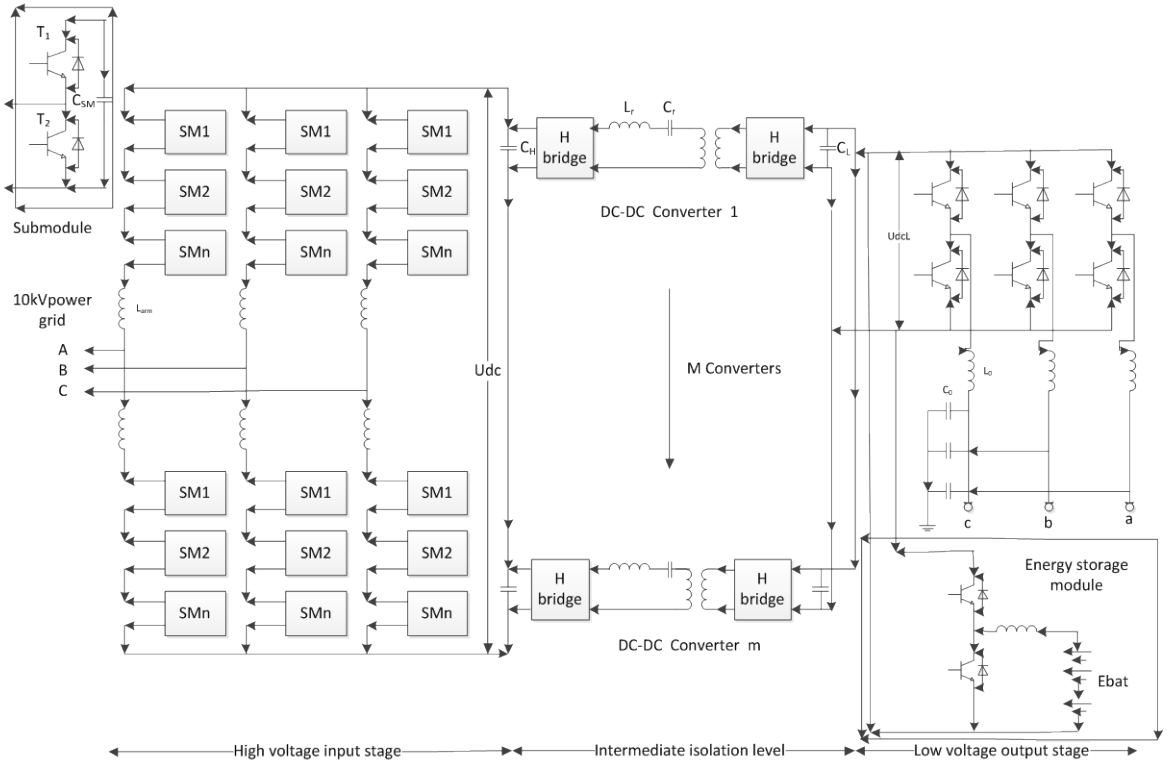

Fig. 1. MMC-structure-based PET topology.

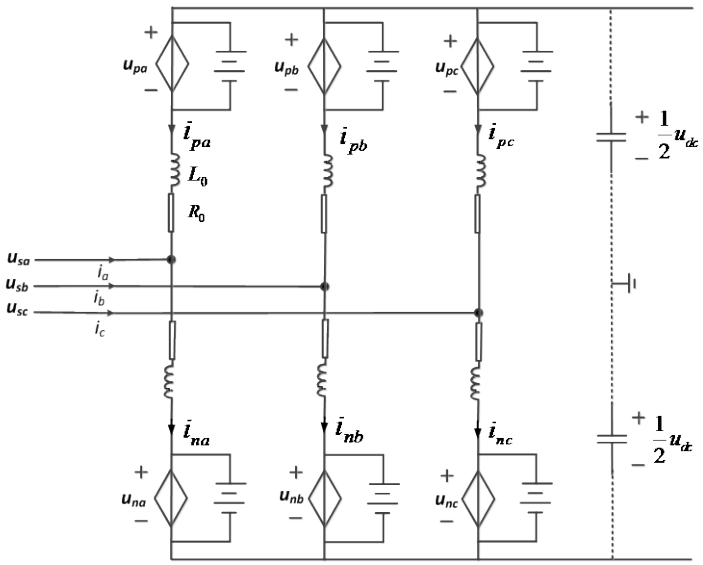

Fig. 2. MMC equivalent circuit diagram.

3. PET MATHEMATICAL MODEL AND CONTROL STRATEGY

3.1 High Voltage Input

3.1.1 MMC Mathematical Model

Figure 2 shows MMC equivalent circuit. The MMC mathematic model will be analyzed according to Figure 2.

As shown in Figure 2, KVL yields:

$$\begin{cases} u_{ca} = \frac{1}{2}u_{dc} - u_{pa} = u_{na} - \frac{1}{2}u_{dc} = \frac{1}{2}(u_{na} - u_{pa}) \\ u_{cb} = \frac{1}{2}u_{dc} - u_{pb} = u_{nb} - \frac{1}{2}u_{dc} = \frac{1}{2}(u_{nb} - u_{pb}) \\ u_{cc} = \frac{1}{2}u_{dc} - u_{pc} = u_{nc} - \frac{1}{2}u_{dc} = \frac{1}{2}(u_{nc} - u_{pc}) \end{cases} \quad (1)$$

where u_{ca}, u_{cb}, u_{cc} represents the voltage to the ground at the points of A, B and C, respectively; u_{pi}, u_{ni} (i=a, b, c) represents the upper arm voltage and lower arm voltage; u_{dc} represents the voltage at the high-voltage DC side.

Therefore,

$$\begin{cases} L\frac{di_a}{dt} + Ri_a = u_{sa} - u_{ca} \\ L\frac{di_b}{dt} + Ri_b = u_{sb} - u_{cb} \\ L\frac{di_c}{dt} + Ri_c = u_{sc} - u_{cc} \end{cases} \quad (2)$$

In the equations, i_a, i_b and i_c represents the three-phase current at the high-voltage AC side; u_{sa}, u_{sb} and u_{sc} represents the three-phase voltage at the high-voltage side. L is the MMC equivalent joint inductance and L_0 is the MMC arm reactor inductance with $L = 0.5L_0$; R is the MMC arm equivalent resistance with $R = 0.5R_0$

After dq transformation, the above equation turns into:

$$\frac{d}{dt}\begin{bmatrix} i_{sd} \\ i_{sq} \end{bmatrix} = \frac{1}{L}\begin{bmatrix} R & -\omega L \\ \omega L & R \end{bmatrix}\begin{bmatrix} i_{sd} \\ i_{sq} \end{bmatrix} + \frac{1}{L}\begin{bmatrix} u_{sd} \\ u_{sq} \end{bmatrix} - \frac{1}{L}\begin{bmatrix} u_{cd} \\ u_{cq} \end{bmatrix} \quad (3)$$

where, i_{sd}, i_{sq}, u_{sd}, u_{sq}, u_{cd} *and* u_{cq} represent the MMC AC-side current, system voltage and the components of MMC AC-side equivalent output voltage at axis d and axis q.

3.1.1 Input Control Strategy

PET input is directly connected to the distribution network and its major function is to realize the the flexible control of the network power factor, the sinusoidal three-phase AC input current and constant DC voltage output at the high-voltage side. The high-voltage AC side adopts the voltage current double closed-loop control. Besides, to reduce the interaction of current at axis d and q in the dynamic process, the step of feed forward decoupling is introduced. Based on the analysis above, the input control is shown in Figure 3.

Each submodule of the MMC contains a capacitor, and it is also necessary to consider the balance of the capacitor voltages among the submodules with the adoption of the sequence-based MMC submodule average voltage control. The exact implementation was demonstrated in the Literature [13].

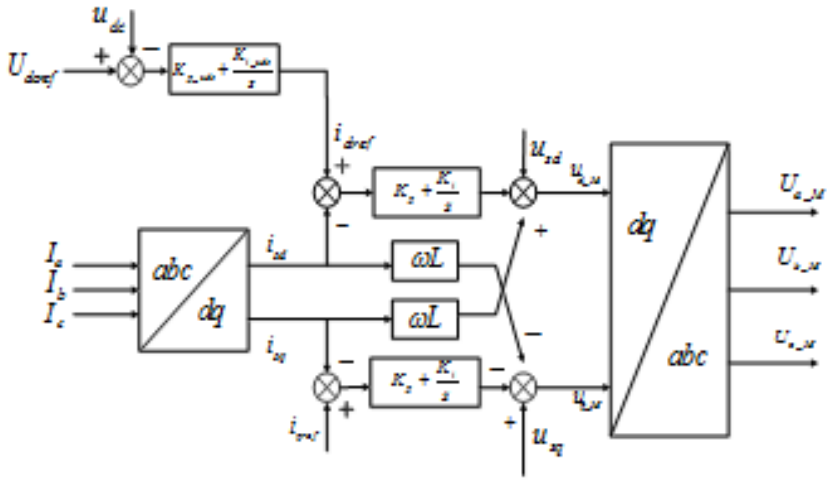

Fig. 3. PET input control.

3.2 Intermediate Isolation

The isolation level adopts the open-loop control and the control process is as follows: the DC signal output from the input step is modulated into high-frequency signal through the original H-bridge and the high-frequency signal is coupled to the secondary by a high-frequency transformer and sent another group of H-bridge convertor, turning the high-frequency signal into DC signal. The control signal of the two H-bridges in this control strategy are the same. This method could easily control the system and the synchronization could be also easily realized.

3.3 Low Voltage Output

The low-voltage output consists of a DC/AC inverter and an LC filter branch. Its major function is to provide the expected voltage waveform to the load, to ensure the normal load power supply. In the occasions with low requirements for system performance, usually the single voltage closed-loop control system can be used [14]. Similar to the input stage, the output stage in the paper chooses the double closed-loop control strategy of voltage and current to realize a better controlling performance. The controlling process is shown in Figure 4.

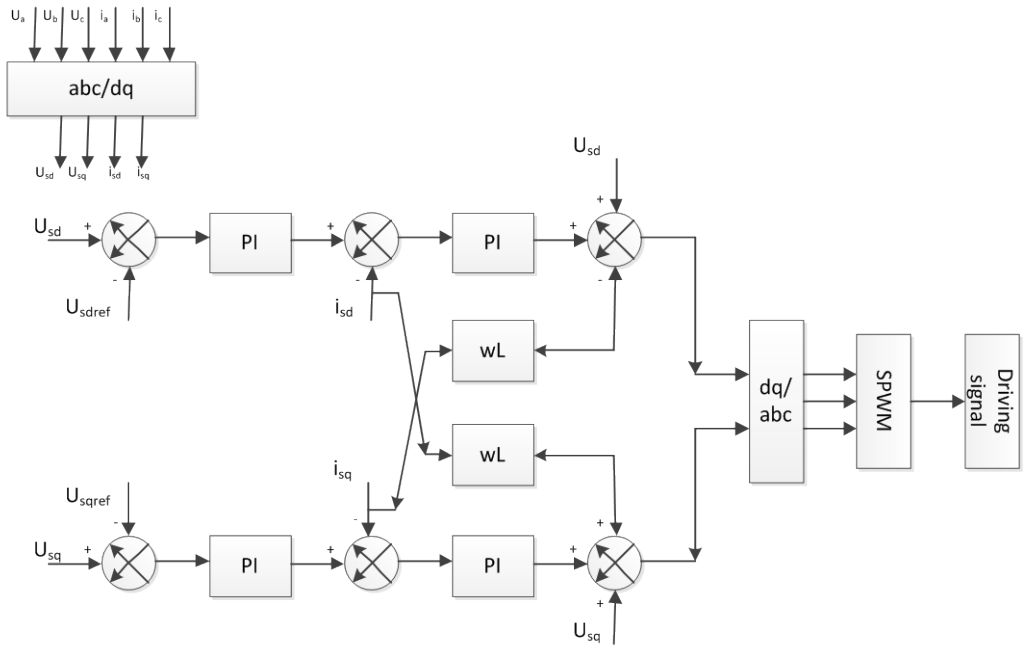

Fig. 4. PET output control.

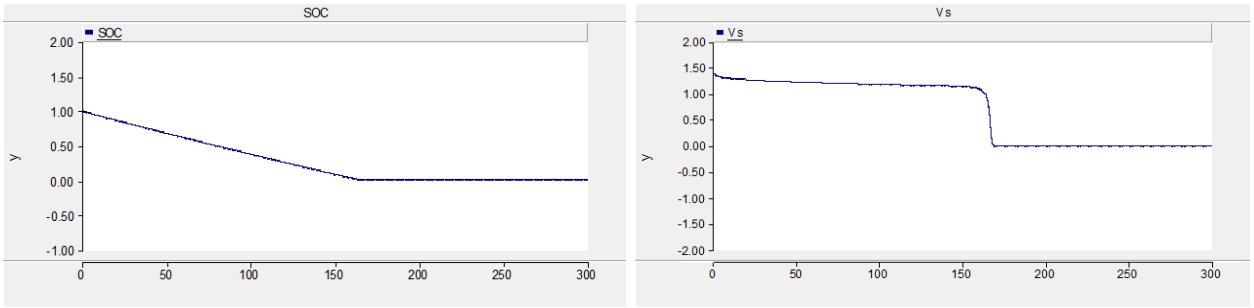

Fig. 5. Battery charging and discharging waveform of voltage and SOC.

3.4 Energy Storage Module

3.4.1 Simulation Model Study

The lithium battery PSCAD simulation model in the paper was based on the compound experience formula mode that is:

$$E = E_0 - RI_{bat} - \frac{k_1}{SOC} - k_2 SOC + k_3 \ln(SOC) + k_4 \ln(1 - SOC) \quad (4)$$

where E_0 is the electromotive force of the battery when SOC is 100%; R is the battery resistance; I_{bat} is the current of real-time charging and discharging of battery; k_1, k_2. k_3 and k_4 are the modification factors.

In the simulation model, the battery is simplified as a series connection of a resistor and the controlled voltage source. In the simulation analysis of the model, E0 is set to be 1.4V and the internal resistance R is 0.1Ω. The simulated charging and discharging waves of the battery is shown in Figure 5. Figure 5a) shows the voltage waveform of the battery. The abscissa is the time in s and the ordinate is the battery voltage (V); Figure 5b) shows the curve of the battery's state of charge (SOC). The abscissa is the time in unit s and the ordinate is the battery's state of charge. It can be seen that the curve of the battery-end voltage during discharge matches the trend and shape of the actual curve in Literature 0, indicating the correctness of the model.

3.4.2 The Influence of Lithium Battery's Energy Storage on the Load Power Supply

After the energy storage system is incorporated into PET, if the grid side fails, the normal power supply of

the load in the subsequent stage could be still guaranteed. This has been described in the Literature [9]-[11] that needs no further explanation. Considering the state of charge (SOC) of the lithium battery, the length of power supply by lithium battery is also one of the factors to be highlighted. The length of the discharge time is directly related to whether the energy storage system can ensure the reliability of the load during the grid fault. Lithium battery discharge time is related to battery capacity, discharge current, temperature, battery resistance and many other factors. The paper mainly discussed the influence of battery capacity on the battery discharge time. In Figure 10, when the battery capacity is rated capacity, the discharge time is about 170s. When the battery capacity is reduced to 80%, as shown in Figure 6 (the abscissa represents time in unit s, and the ordinate represents the battery state of charge), the discharge duration is reduced to about 133s. Therefore, when other conditions remain the same, the larger the battery capacity, the longer the discharge time.

Literature [16] pointed out that the actual battery discharge capacity is affected by temperature, discharge rate and other factors. Among them, the discharge capacity of the lithium battery at a small discharge rate is larger than the discharge capacity at a large discharge rate. Theoretically, the higher the temperature is, the more capacity is discharged. However, long-term working of battery in a high-temperature state would shorten the battery life. Therefore, in engineering applications, it is necessary to fully consider the factors such as temperature, discharge rate of lithium battery, and failure time, and configure the lithium battery capacity according to specific conditions to ensure the reliability of the load during grid fault.

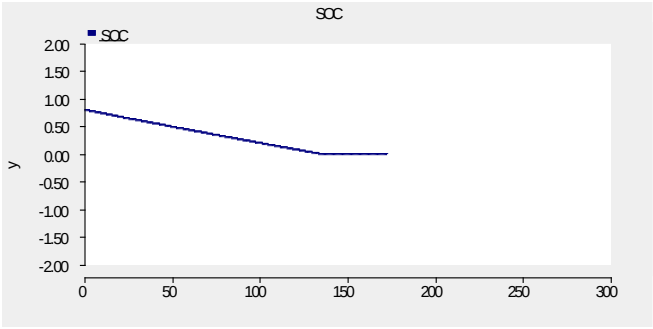

Fig. 6. Battery capacity becomes 80%.

Table 1. The parameters of PET input.

MMC Each phase leg inductance(mH)	28
Sub-module capacitance value(μF)	1000
Sub-module capacitor voltage reference(kV)	2
The number of upper / lower bridge arm modules per phase in MMC	10

Table 2. The parameters of PET isolation.

High side capacitor value(μF)	650
DC-DC Converter resonant inductor(μH)	60
DC-DC Converter resonant capacitor(μF)	11.7
High frequency transformer rated ratio	2000:750
Low side capacitor value(μF)	450
DC/DC Number of converters	10

Table 3. The parameters of PET output.

Filter capacitor(μF)	550
Filter inductance(mH)	100
Low side load power(MVA)	0.5
Load power factor	0.8
Load Resistance(Ω)	0.23
Load inductance(mH)	0.55

4. SIMULATION RESULT AND ANALYSIS

To verify the proposed topology and the feasibility of adopted control strategy, a PET simulation model was established in the PSCAD simulation environment for analysis and verification. Among them, the rated voltage of the grid is 10kV, the rated capacity of the system is set to 5MVA, the reference voltage of the high voltage

DC side of PET is 20kV, the low voltage DC side voltage is 0.75kV and the low voltage output side AC voltage is 0.38kV. Specific simulation parameters are listed in Table 1 to Table 3.

In the simulated waveform given below, the abscissa is time in unit s; the ordinate of the voltage current wave form is voltage value (kV) and current value (kA).

4.1 Simulation of Steady-State Operation

Figure 7 shows the steady-state PET simulation results, in which the low-voltage output side load power factor is 0.8. As can be seen from Figure 7a), the voltage and current at the input side can basically maintain the same phase. The measured input power factor is close to 1, and the control strategy adopted can ensure the unit power operation on the input side. At the same time, it can be seen from the simulation results in Figure 7b) that PET has good output characteristics under steady-state operation and the total voltage distortion of the measured voltage is about 2.8%. Simulation results show that the control strategy adopted in steady-state operation makes PET have good input and output characteristics.

4.2 Load Input

Figure 8 shows the simulation results from non-load to load of PET. PET is started with no load and the load is added when t = 0.6s. It can be seen from Figure 8 that the load changes abruptly but there is no obvious change in the voltage and current waveforms at the input stage. After measurement, the high-voltage side keeps running at high power factor. As shown in Figure 8b), the output voltage suddenly fluctuates; however, the fluctuation time is very short and resumes stable operation after about 0.01s. The response speed is obviously faster than the result in the Literature [14]. The above results show that under sudden load changes, PET can resist load disturbances and the dynamic response remains quick enough.

4.3 Fault Operation

Figure 9 and Figure 10 show the simulation results of 10kV AC side three-phase voltage and load-side three-phase voltage when the three-phase grounding fault and the single-phase grounding (A-phase grounding) fault occurred on the load side. Among them, the fault occurred at t = 0.6s and lasted for 0.05s. It can be seen from the simulation results in Figure 9 that the three-phase voltage instantaneously drops to zero when the three-phase grounding fault occurs on the load side and the voltage returns to normal after about 0.02 seconds after the fault is rectified. The three-phase AC voltage of the high-voltage side has not changed during the entire fault. As can be seen from Figure 10, a single-phase grounding fault on the load side has no effect on the grid voltage. The results show that PET has the ability to isolate fault propagation and prevent the range of faults from expanding.

4.4 Harmonics Simulation

Figure 11 shows the simulation results of the three-phase voltage on the 10kV AC side and the three-phase voltage on the output side when the load side voltage gained three times and five times of harmonics. From Figure 11, it can be seen that in the case of harmonics on the load side, the voltage still maintains a three-phase sinusoidal variation, independent of the load-side harmonics. Simulation results show that PET has the ability of isolating harmonic propagation.

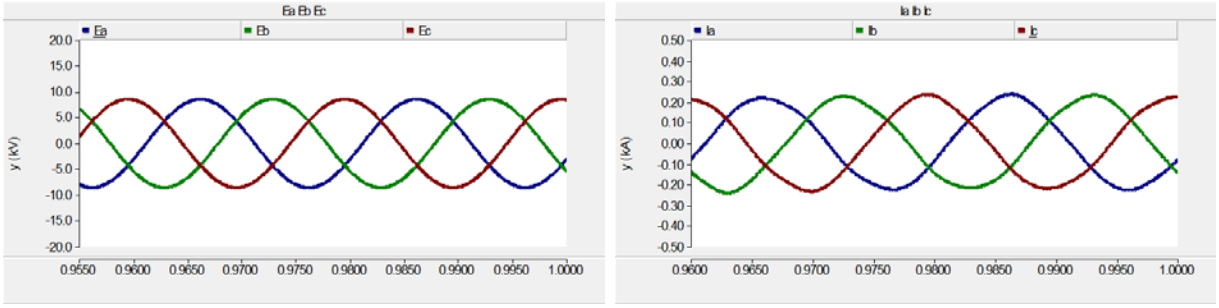

a) simulation of 10kV AC side three-phase voltage and current

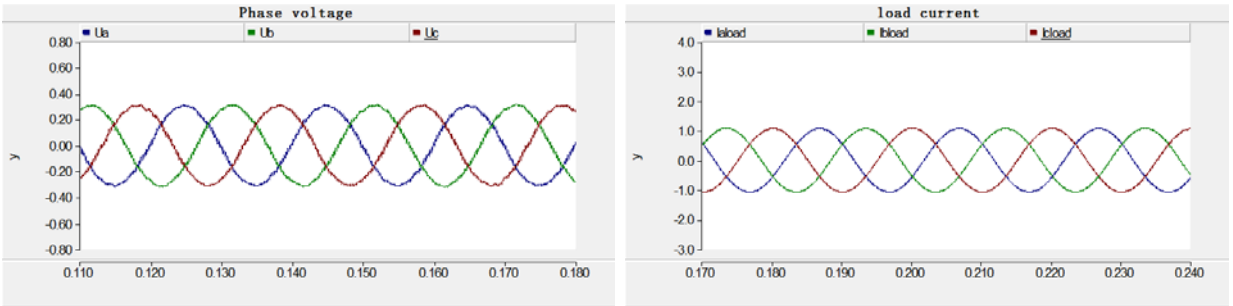

b) Simulation of low voltage side three-phase voltage and current.

Fig. 7. Simulation results of steady state operation.

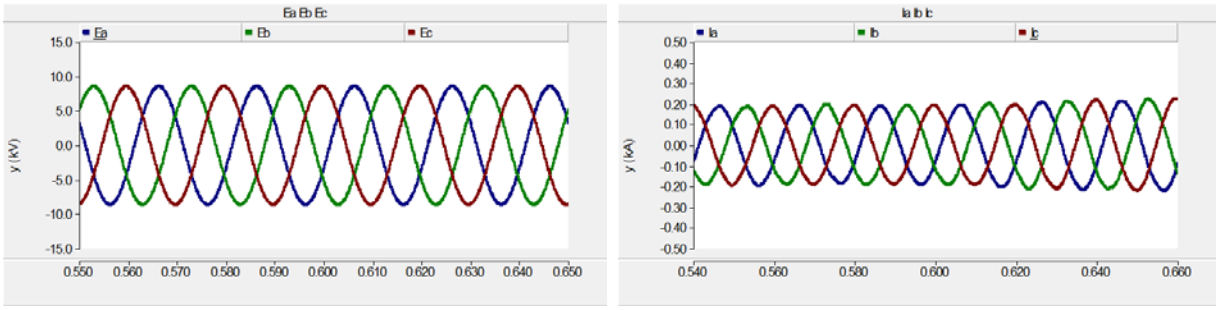

a) simulation of 10kV AC side three-phase voltage and current

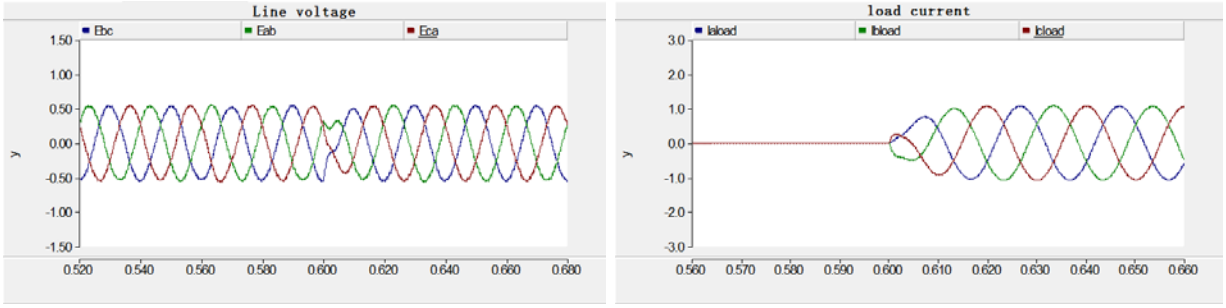

b) Simulation of low voltage side three-phase voltage and current.

Fig. 8. Influence of load change.

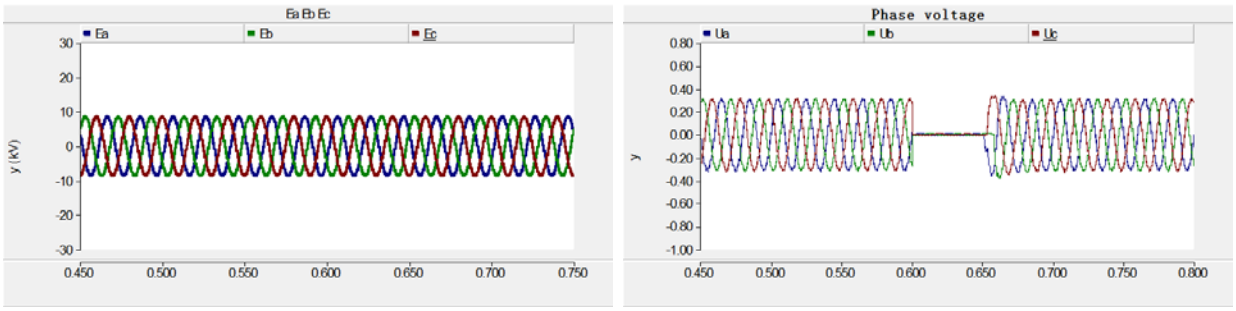

Fig. 9. Simulation results of three phase grounding fault on load side.

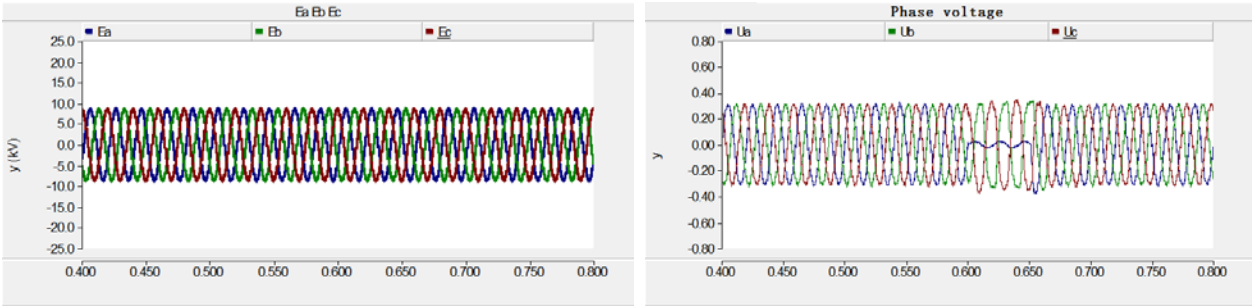

Fig. 10. Simulation results of single phase grounding fault on load side.

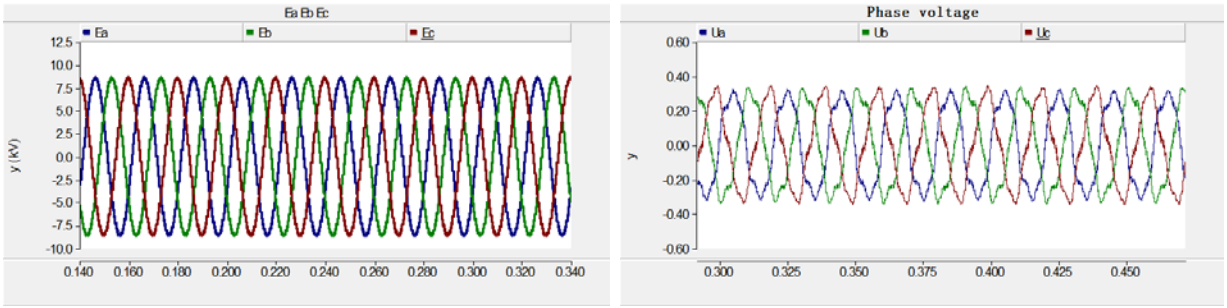

Fig. 11. Load side voltage adding 3rd and 5th harmonics.

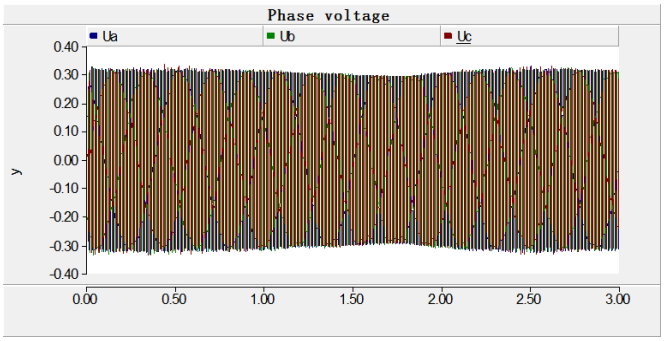

Fig. 12. Voltage waveform in load side of input voltage interruption.

4.5 Voltage Interruption

Figure 12 shows the load side voltage waveform at the voltage interruption on the 10kV AC side. The voltage interrupt occurred at t=0.5s and lasted for 2s. It can be seen from Figure 12 that when the input voltage is interrupted, the energy storage system can support the load and ensure the normal power supply of the load.

5. CONCLUSION

Power electronic transformer has outstanding characteristics, and remains consistent with needs of smart grid's future development. It is expected to be widely used in the distribution networks. The paper put forward the topology combining PET with lithium battery energy storage, which ensures both the quality and reliability of the load power supply, suggesting a high research value.

ACKNOWLEDGEMENTS

This work was supported by the National Key R&D plan (2016YFD0702103 and 2017YFD0710201), Shandong province natural science foundation of China (2015ZDZX10002, 2017GGX30105 and 2017CXGC080), Innovation plan of agricultural machinery and equipment in Shandong province No. 2017YF006-02.

REFERENCES

[1] Peng Q., Dongmei S., and Baojian J., 2016. Research on smart distribution grid oriented power electronic transformer. *Electrical Measurement and Instrumentation* 53(1): 112-116.

[2] Guohu L., Guoyue Q., and Xufeng Y., 2014. Summary of the power transformer research. *Electrical Measurement and Instrumentation* 51(16): 5-12.

[3] Yanyan D., 2015. Studies on solid state transformer and its control strategies. Jinan:Shandong University.

[4] Zhendong J., Dongye L., and Yichao S., 2016. Research on a three-phase cascaded power electronic transformer and its control strategy. *Electric Machines and Control* 20(8): 32-40.

[5] Zixin L., Ping W., and Zunfang C., 2013. Research on medium and high-voltage smart distribution grid oriented power electronic transformer. Power System Technology 37(9): 2592-2601.

[6] Guangxing S., Ruifeng G., and Wei S., 2016. Research on topology and control strategy of power electronic transformer based on MMC structure. *High Voltage Apparatus* 52(1): 142-148.

[7] Jiye H., Yong L., and Yijia C., 2016. A new modular multilevel type solid state transformer with internal model control method (in Chinese). *Sci Sin Tech* 46: 518–526.

[8] Jiaping Z., Li S., and Hua C., 2014. Research on power electronic transformer with energy storage system used in intelligent distribution network. *Electric Technology* 33(5):7 4-78.

[9] Haibo L., Chengxiong M., and Jiming L., 2010. Energy storage system of electronic power transformer and its optimal control. *Transactions of China Electrotechnical Society* 25(3): 54-60.

[10] Liang M., Qianshuang W., and Zhiqiang G., 2014. Economic operation analysis on energy storage battery in microgrid. *Electrical Measurement and Instrumentation* 51(10): 120-124.

[11] Yang L., Research of solid state transformer application in smart grid. Jinan: Shandong University.

[12] Tiejun Z., Jianzheng L., and Jingwei G., 2011. The design of high-power PWM rectifie. *Electrical Measurement and Instrumentation* 48(6): 85 -87.

[13] Zheng X., Qingrui T., Minyuan G., 2012. Flexible direct current transmission system. Beijing: China Machine Press.

[14] Guohu L, Xufeng Y., and Guoyue Q., 2014. Research on the simulation of the power electronic transformer in the distribution network. *Electrical Measurement and Instrumentation* 51(17): 35-41.

[15] Maharjan L., Inoue S., Akagi H., and Asakura J., 2009. State-of-charge (SOC)-balancing control of a battery energy storage system based on a cascade PWM converter. *IEEE Transactions on Power Electronics* 24(6): 1628-1636.

[16] Wenzheng D., Zengxin W., and Pei T., 2011. Modeling of electrical characteristics of lithium iron phosphate battery. *Yunnan Electric Power* 39(6): 54-56.